A Direct Discrete Complex Image Method From the Closed-Form Green's Functions in Multilayered Media

Mengtao Yuan, *Student Member, IEEE*, Tapan K. Sarkar, *Fellow, IEEE*, and Magdalena Salazar-Palma, *Senior Member, IEEE*

***Abstract*—Sommerfeld integration is introduced to calculate the spatial-domain Green's functions (GF) for the method of moments in multilayered media. To avoid time-consuming numerical integration, the discrete complex image method (DCIM) was introduced by approximating the spectral-domain GF by a sum of exponentials. However, traditional DCIM is not accurate in the far- and/or near-field region. Quasi-static and surface-wave terms need to be extracted before the approximation and it is complicated to extract the surface-wave terms. In this paper, some features of the matrix pencil method (MPM) are clarified. A new direct DCIM without any quasi-static and surface-wave extraction is introduced. Instead of avoiding large variations of the spectral kernel, we introduce a novel path to include more variation before we apply the MPM. The spatial-domain GF obtained by the new DCIM is accurate both in the near- and far-field regions. The CPU time used to perform the new DCIM is less than 1 s for computing the fields with a horizontal source-field separation from $1.6 \times 10^{-4}\lambda$ to 16λ. The new DCIM can be even accurate up to 160λ provided the variation of the spectral kernel is large enough and we have accounted for a sufficient number of complex images.**

***Index Terms*—Discrete complex image method (DCIM), matrix pencil method, method of moments (MoM), multilayered media, Sommerfeld integration (SI).**

I. Introduction

COMPUTATIONAL electromagnetics (CEM) has evolved rapidly since the 1960s with the increase of the computational power of computers. Among the various CEM methods, the method of moments (MoM) [1] is extensively studied. The MoM is a variational method sometimes based on integral equations. It requires segmentation of the structure only on the surface and no absorbing boundary condition (ABS) is necessary. Hence, it is more robust and concise and is preferred to be used for most open structures radiating in free space. The Green's function (GF) from the source element to the field element is required to evaluate the impedance matrix. However, for structures located in multilayered media, such as the real ground plane of the earth and the stratified structure of printed or integrated circuits, the GFs used in the MoM are different and much more complicated to derive than those for free space. Moreover, the Sommerfeld integration (SI) [2] is introduced to the calculation of the spatial-domain s, which is very time consuming [3] and complicated [4].

The discrete complex image method (DCIM) was developed to avoid the numerical computation of the SI [5]–[9]. Using the generalized pencil of functions (GPOF) matrix method, closed form can be obtained without any numerical integration. In [5], the quasi-static (which contributes in the near-field region) and surface-wave terms (which contribute in the far-field region) are extracted first. The spectral domains are then approximated by a sum of complex exponentials that contribute in the medium distance region. The closed forms in the spatial domain are then obtained analytically by the use of the Sommerfeld identity. A two-level DCIM without a surface-wave extraction is proposed in [6] to save the number of samples of the spectral-domain GF. The DCIM in the k_ρ-plane (k_ρ is the radial wavenumber) is introduced in [8], but z or z' cannot be extracted from the spectral-domain GF to simplify the computation. The traditional DCIM without the surface-wave extraction has a large error in the far-field region due to the fact that the traditional DCIM does not contain enough information for the surface-wave poles. For a general multilayered case, the surface-wave terms cannot be obtained analytically. The extraction of the surface-wave components numerically is complicated ([7] and [9]). Even with the surface-wave poles extracted, errors occur for the near-field region due to the singularity at the origin for Hankel functions when $z \neq z'$ [7]. Correction terms have to be used to compensate for this singularity in the near-field region [9]. As a summary, the methods that avoid the numerical computation of the SI can save time during the matrix filling step of the MoM, but have their disadvantages or difficulties on surface-wave extractions and have different forms of expressions for the spatial domains.

The following two features of the GPOF method [10] (a better approach is the matrix pencil method in [11]) have been neglected or misunderstood by the previous authors in employing DCIM.

- Although only several samples of a function on a finite path are used to implement the matrix pencil method (MPM), the MPM tries to fit this function on the whole complex plane.
- The MPM has the capability to fit functions with large variations.

Manuscript received June 2, 2005; revised September 16, 2005.

M. Yuan and T. K. Sarkar are with the Department of Electrical Engineering and Computer Science, Syracuse University, Syracuse, NY 13244 USA (e-mail: myuan@syr.edu; tksarkar@mailbox.syr.edu).

M. Salazar-Palma is with the Departamento de Señales, Sistemas y Radiocomunicaciones, Universidad Politécnica de Madrid, Madrid 28040, Spain (e-mail: Salazar@gmr.ssr.upm.es).

Digital Object Identifier 10.1109/TMTT.2005.864138

The information of singularities of the functions can be obtained by MPM if the parameters are properly chosen.

In this paper, we propose a direct DCIM without any quasi-static or surface-wave terms extracted. A novel path is chosen to obtain sufficient information of both the singularities and the trend of the spectral domain GF to infinity. Hence, the discrete complex images (DCIs), which were supposed to approximate the spatial domain GFs only in medium distance region, can be also accurate both in near and far field regions. Simulation results show this direct DCIM can get closed-form spatial domain GF from $1.6 \times 10^{-4}\lambda$ to 160λ. The large distance up to 160λ is sufficient for extremely large structures analyzed in MoM. Another merit of this direct DCIM is that the closed-form GF is expressed by a sum of exponential functions divided by a distance, which is similar to the GF of spherical waves in homogeneous media, which makes computer programming much simpler. The numerical techniques for the matrix filling step of MoM in homogeneous media can be directly used for the multilayered media.

II. Traditional DCIM and Discussions

Suppose only electric currents are present, the mixed-potential integral equation (MPIE in [12]) representation for $\mathbf{E}$ in an inhomogeneous media can be expressed as

$$\begin{aligned}\mathbf{E} &= -j\omega\mathbf{A} - \nabla\Phi \\ &= -j\omega\mu_0\langle\underline{\mathbf{G}}^A;\mathbf{J}\rangle + \frac{1}{j\omega\varepsilon_0}\nabla\left(\langle K^\Phi, \nabla'\cdot\mathbf{J}\rangle + \langle C^\Phi\hat{z};\mathbf{J}\rangle\right).\end{aligned} \tag{1}$$

The bold letters in (1) mean vectors. $\underline{\mathbf{G}}^A$ is the vector potential dyadic Green's function (DGF) in spatial domain where the underline means 'dyadic'. K^Φ is the scalar potential kernel and C^Φ is the correction factor, which arises when $\nabla\cdot\underline{\mathbf{G}}^A$ cannot be simply expressed by $\nabla' K^\Phi$ as in layered media. $\langle\bullet\rangle$ is the integration over the source region where $\mathbf{J}$ exists. The spatial domain DGF $\underline{\mathbf{G}}^A$ can be expressed as

$$\underline{\mathbf{G}}^A = \begin{bmatrix} G^A_{xx} & 0 & 0 \\ 0 & G^A_{yy} & 0 \\ G^A_{zx} & G^A_{zy} & G^A_{zz} \end{bmatrix}. \tag{2}$$

We use $f(\boldsymbol{\rho};z|z')$ to express each component of this dyadic, K^Φ or C^Φ. The spatial domain $f(\boldsymbol{\rho};z|z')$ can be obtained through SI from the *spectral-domain GF* $\tilde{f}(k_\rho;z|z')$

$$f(\boldsymbol{\rho};z|z') = \int_0^\infty \tilde{f}(k_\rho;z|z')J_\nu(k_\rho\rho)k_\rho dk_\rho, \qquad \nu = 0,1 \tag{3}$$

where J_n is the first kind Bessel function of order n. Although (1)–(3) are applicable to uniaxially anisotropic media, in this paper we focus on stratified isotropic media.

The spectral domain GF $\tilde{f}(k_\rho;z|z')$ can be obtained by the equivalent transmission-line Green's functions (TLGF) expressed through voltages and currents [12]. Since the stratified media can be easily modeled as transmission-line sections, the voltages and currents can be obtained by the known sources together with the reflection and transmission coefficients.

When $\nu = 0$, also the source and field points are in the same layer, the SI can be written as

$$\begin{aligned}f(\boldsymbol{\rho};z|z') &= \frac{e^{-jkr_0}}{jkr_0} + \int_0^\infty \tilde{f}(k_\rho;z|z')J_0(k_\rho\rho)k_\rho dk_\rho \\ &= \frac{e^{-jkr_0}}{jkr_0} + \int_0^\infty \frac{e^{-jk_z|z+z'|}}{jk_z}\tilde{G}(k_\rho)J_0(k_\rho\rho)k_\rho dk_\rho\end{aligned} \tag{4}$$

where $r_0 = \sqrt{\rho^2 + (z-z')^2}$ is the direct line from the source point to the field point. We call $\tilde{G}(k_\rho)$ the spectral kernel of the GF. k_ρ and k_z are related by

$$k_\rho^2 + k_z^2 = k^2 \tag{5}$$

where k is the wavenumber in the layer to be analyzed. Suppose $\tilde{G}(k_\rho)$ can be approximated as

$$\tilde{G}(k_\rho) \cong \sum_{i=1}^{M} a_i e^{-b_i k_z} \tag{6}$$

by the MPM. We also have the Sommerfeld identity

$$\int_0^\infty \frac{e^{-jk_z|z|}}{jk_z}J_0(k_\rho\rho)k_\rho dk_\rho = \frac{e^{-jkr_1}}{r_1}. \tag{7}$$

Note that if $\nu = 1$ in (3), we can use the derivative of the Sommerfeld identity (7), which is

$$\int_0^\infty \frac{e^{-jk_z|z|}}{jk_z}J_1(k_\rho\rho)k_\rho^2 dk_\rho = (1+jkr_1)\frac{\rho e^{-jkr_1}}{r_1^3}. \tag{8}$$

The process of DCIM for $\nu = 1$ is similar to that for $\nu = 0$. In this paper, we focus on the situation when $\nu = 0$. From (7) we have

$$\begin{aligned}f(\boldsymbol{\rho};z|z') &\cong \frac{e^{-jkr_0}}{jkr_0} \\ &\quad + \int_0^\infty \sum_{i=1}^{M} a_i \frac{e^{-jk_z(|z+z'|-jb_i)}}{jk_z}J_0(k_\rho\rho)k_\rho dk_\rho \\ &= \frac{e^{-jkr_0}}{jkr_0} + \sum_{i=1}^{M} a_i \frac{e^{-jkr_i}}{r_i}.\end{aligned} \tag{9}$$

The spatial domain GF can be expressed as a sum of GFs by the direct source and the N image sources located at complex distances $r_i = \sqrt{\rho^2 + (z+z'-jb_i)^2}$ in homogeneous media.

If the source point is in layer m, the field point in layer n and $m \neq n$, there will be two wavenumbers k_{zm} and k_{zn} associated with z' and z respectively. z' and z are difficult to be decomposed from $\tilde{f}(k_\rho;z|z')$. In this situation, we choose $\tilde{f}(k_\rho) = \tilde{G}(k_\rho;z,z')/jk_z$ and apply GPOF on $\tilde{G}(k_\rho;z,z')$ [7]–[9]. Without loss of generality of $\tilde{G}(k_\rho;z,z')$ and for an easier analysis, we suppose $m = n$ and use $\tilde{G}(k_\rho)$ in (4) as the spectral kernel.

Since the matrix pencil method (MPM) is applicable for a complex function with a real variable and the functions should

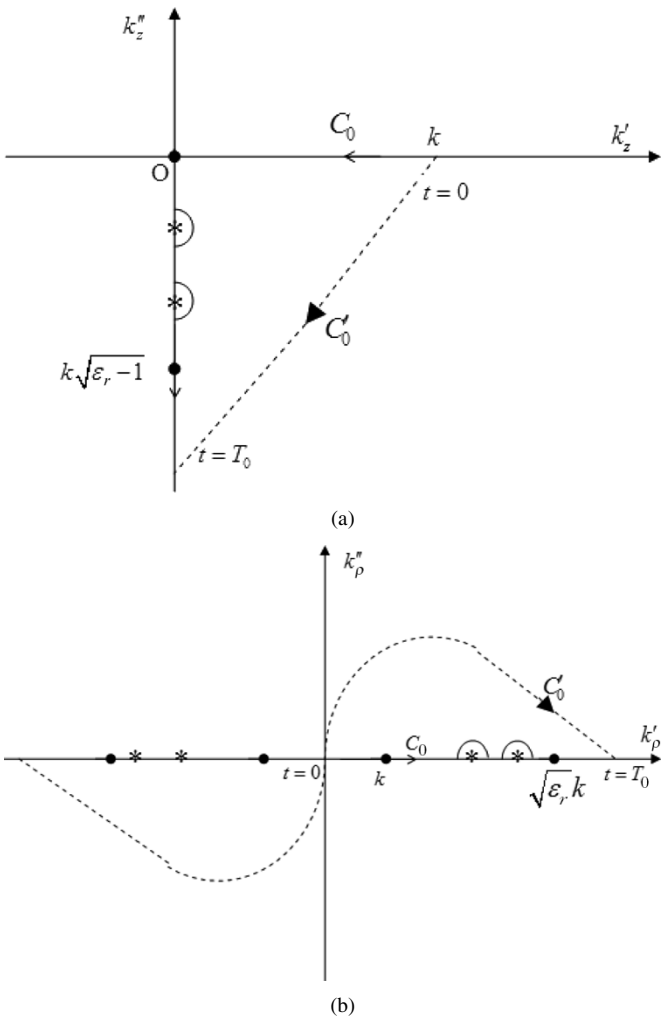

Fig. 1. (a) Path of traditional DCIM in k_z domain. (b) Path of traditional DCIM in k_ρ domain.

be equally sampled along the variable, we choose a path C_0' such as

$$k_z = k\left[-jt + \left(1 - \frac{t}{T_0}\right)\right], \qquad 0 \le t \le T_0. \tag{10}$$

This path is a straight line in the k_z-plane starting from $k_z = k$, as shown in Fig. 1(a), which maps to the origin on the k_ρ-plane, as seen in Fig. 1(b). This path keeps the linear relationship between t and k_z, which is convenient to derive a_i and b_i. It should remain in one Riemann sheet. T_0 should be chosen such that k_z is larger than the branch point $k\sqrt{\varepsilon_r - 1}$ to avoid the singularities (marked as an $*$ in these figures).

As an example, we consider the simple microstrip case for one layer substrate with the dielectric constant $\varepsilon_r = 12.6$ and thickness $h = 1$ mm, as shown in Fig. 2 [5]. The spectral kernel $\tilde{G}_q$ for the scalar potential GF due to a horizontal dipole along path C_0' with t is shown in Fig. 3. The dots are the data recovered by the MPM. In this example, the frequency $f = 30$ GHz and $T_0 = 15$. $\tilde{G}_q$ in Fig. 3 is equivalent to K^Φ in (1). Both here and in Section III, for demonstration purposes, we will use $\tilde{G}_q$. We apply and use the same DCIM for all the components in (1).

Note that the static term is not extracted as before where we apply the MPM ($\lim_{t\to\infty} \tilde{G}_q \neq 0$). Moreover, we do not use the

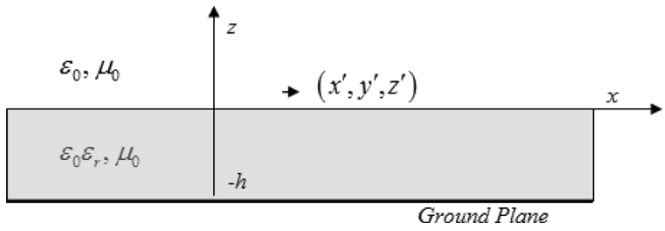

Fig. 2. Microstrip structure.

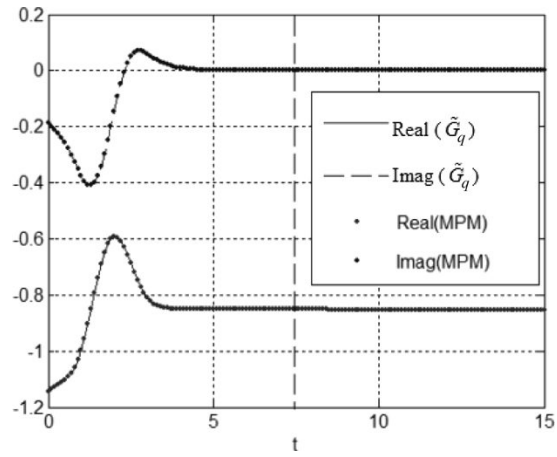

Fig. 3. $\tilde{G}_q$ sampled along path C_0' in Fig. 2.

samples of $\tilde{G}_q$ from $t = 0$ to $t = T_0$. Instead we use the samples to the left-hand side of the vertical line ($t = 7.5$). The MPM can estimate the remaining data (from $t = 7.5$ to $t = 15$) well, as shown in Fig. 3.

The spatial-domain GF including the direct term can be written as

$$G_q = \frac{\mu_0}{4\pi}\left(\frac{e^{-jkr_0}}{r_0} + \int_0^\infty \frac{e^{-jk_z|z+z'|}}{jk_z}\tilde{G}_q J_0(k_\rho\rho)k_\rho dk_\rho\right). \tag{11}$$

A plot of G_q is shown in Fig. 4. The dots are the G_q computed by the DCIM, while the line is the accurate result obtained by direct numerical integration [4]. From Fig. 4, we can see that the DCIM is accurate for small and medium values of ρ. However, it blows up for large ρ. The reason is that the surface-wave term is not extracted and it contributes to the far-field component (see [7] and [9]). The surface-wave term from the singularities can be written as

$$G_q^{\text{sw}} = \frac{1}{4\pi}\left(-2\pi j\sum_i \text{Res}_i H_0^{(2)}(k_{\rho i}\rho)k_{\rho i}\right) \tag{12}$$

due to the Gaussian integration theorem. Res_i is the residue for the corresponding singularity $k_{\rho i}$. Computation of the surface-wave term includes the evaluation of the Hankel function. Very small values of ρ are close to the singularity of the Hankel function, which does not naturally exist in the spatial GF when $z \neq z'$. Hence, error occurs in the near-field region [7]. Extra effort has to be done to compensate for this error if we want one GF to remain for both the near- and far-field regions [9]. Moreover, the locations of the singularities are difficult to find, especially for general multilayered media. Some complicated

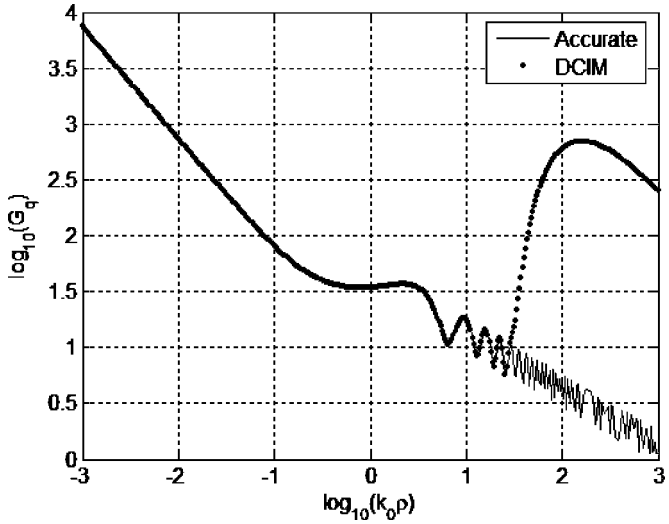

Fig. 4. Spatial-domain G_q obtained by traditional DCIM.

numerical techniques have been proposed to locate the singularities in [7] and [9]. Even if the singularities are accurately located, the form in (12) is different from (9), which destroys the advantages of using a single simple expression for the spatial-domain GF.

III. New Direct DCIM

Extra effort has been made to compensate in the DCIM, as shown in [5]–[9], because the capability of the MPM is not fully recognized and implemented. As described in Section II, it is not necessary to extract the static term or to make $\tilde{G}_q$ near to zero at $t = T_0$. The MPM can estimate the behavior of $\tilde{G}_q$ out of the path provided sufficient variation information is included in the path. Theoretically speaking, if we have arbitrary accuracy (an infinite number of significant digits) for the computation and the sample values used in the MPM, the discrete images obtained from the path in Fig. 1 will be sufficient to approximate the spectral kernel in the whole k_z domain, including the surface poles. For the same reason, the traditional DCIM cannot generate an accurate GF in the far field, not because the MPM cannot approximate function with fast variation, but because the path chosen cannot provide sufficient information generated by the singularities. This difficulty is caused by numerical limitation along the original path. With these features of MPM, choice of the path can be more flexible and efficient, and the direct DCIM can obtain satisfactory results without any extra compensation methods.

The first change of the path is to C_2, as shown in Fig. 5. This change is to eliminate the necessity of choosing a slope in the path and to simplify the relationship between t and k_z as follows:

$$k_z = k[-jt + 1], \qquad 0 \le t \le T_0. \tag{13}$$

Another advantage of this change is to make the path parallel to the imaginary axis, around which the singularities are distributed. The nearest distance between the path and different singularities will be the same so that the contribution of each

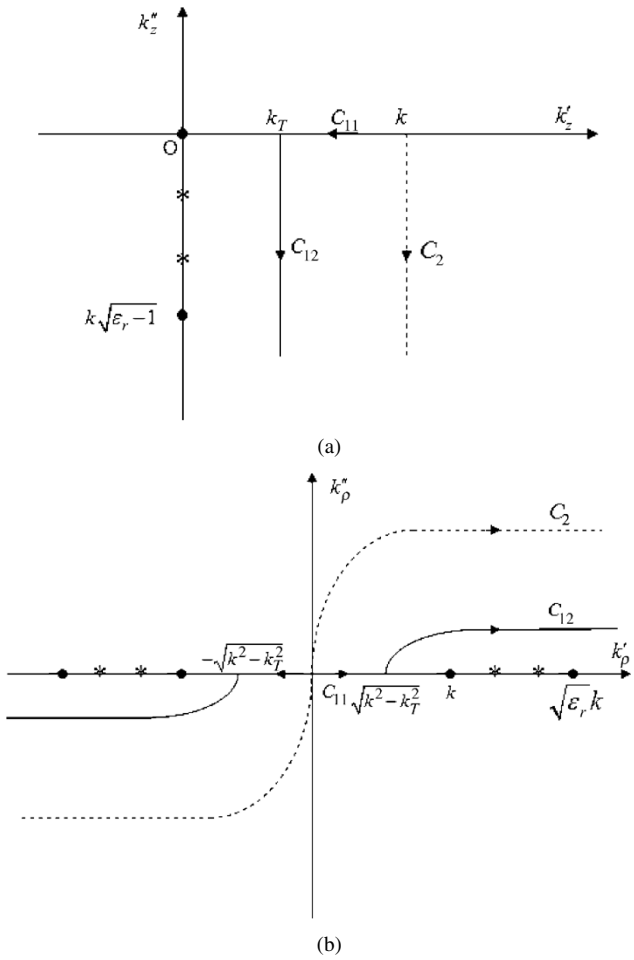

Fig. 5. (a) Path of the new DCIM in k_z domain. (b) Path of the new DCIM in k_ρ domain.

singularity will be equally sampled along the path. Simulation results in Section IV show that the path C_2 can also generate satisfactory results of the spatial GF in the near- and medium-field regions.

The second change of the path is more critical. Researchers involved with the traditional DCIM tried to avoid the large variations of the spectral kernel. In this paper, we do the reverse: we try to include more variations of the spectral kernel before we do the MPM. The idea is implemented by moving the path closer to the singularities, which is shown as path C_{12} in Fig. 5. Suppose we shift the starting point of C_{12} to k_T, where

$$k_T = \gamma k, \qquad 0 < \gamma \le 1. \tag{14}$$

The path of C_{12} is then changed as

$$k_z = \gamma k[-jt + 1], \qquad 0 \le t \le \frac{T_0}{\gamma}. \tag{15}$$

We can get another sequence of values of the spectral kernel. A plot of $\tilde{G}_q$ for $\gamma = 0.1$ is shown in Fig. 6. Compared with Fig. 3, this plot shows large variations due to the singularities, but the MPM can still approximate them well. The two singularities for this example show up in Fig. 6, while we cannot differentiate them in Fig. 3. Simulation results in Section IV show that the proposed DCIM is accurate both in the near- and far-field regions if γ is small enough.

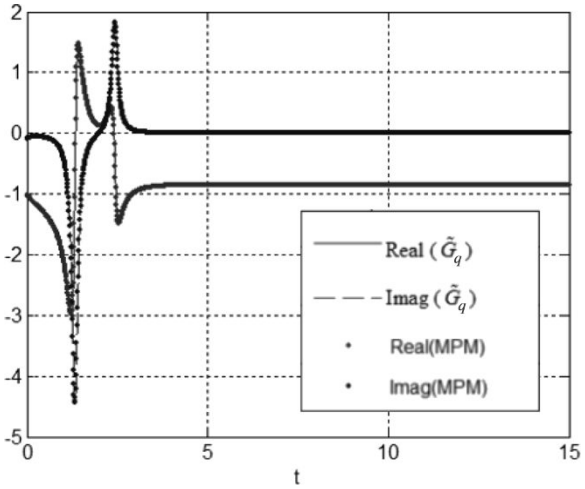

Fig. 6. $\tilde{G}_q$ sampled along path C_{12} in Fig. 5.

One of the main purposes of this paper is to illustrate that the traditional DCIs cannot approximate the spatial-domain GF in the far-field region alone, not because the DCIs have the decay rate of $1/rho$ while the surface-wave poles have a different decay rate of $1/\sqrt{\rho}$, but because we do not have enough exponentials to approximate the special kernel. From a theoretical point-of-view, a continuous function $g(x)$ can be analytically expressed by a Fourier series, which is a special case of exponentials. It is similar that any $\tilde{G}(k_\rho)$ continuous in a specific part of the k_z-plane can be analytically expressed by a series of complex exponentials. Together with the Sommerfeld identity, there should be no theoretical difficulty for DCIs approximating the spatial-domain GF without any singularity extraction.

To make the modified path start from the origin in the k_ρ-plane, we need to sample the spectral-domain kernel along a compensating path C_{11}. The MPM is applied on C_{11} for the remaining variations that are not on C_{12}.

The recipe of the proposed direct DCIM is as follows.

1) Choose the value of γ according to the requirement of the spatial-domain GF. Smaller γ will introduce more variation of the spectral-domain kernel and more information of the singularities. More accurate results can be obtained for smaller γ, especially in the far-field region. This requires more samples for the MPM and more poles will be generated and, hence, the computational load will be increased.
2) Approximate the spectral kernel on path C_{12} as
$$\tilde{G}(k_\rho)|_{C_{12}} \approx \sum_{i=1}^{M} a_i e^{-jb_i k_{z0}}\Big|_{C_{12}}. \tag{16}$$
This step is usually the most time-consuming step for the DCIM. For accurate requirements for the spatial-domain GF, M can be over 100.
3) Approximate the remaining part on path C_{11} as
$$\tilde{G}(k_\rho)|_{C_{11}} - \sum_{i=1}^{M} a_i e^{-jb_i k_{z0}}\Big|_{C_{11}} \approx \sum_{i=1}^{M} a_i' e^{-jb_i' k_{z0}}\Big|_{C_{11}}. \tag{17}$$
As the MPM on C_{12} can estimate the behavior of the spectral kernel on C_{11}, the values of (17) should be very small. To approximate the remaining variations, 5–8 poles of the MPM are enough.
4) The spatial-domain GF can be expressed as
$$G(\rho, z|z') = \frac{e^{-jk_0 r_0}}{r_0} + \sum_{i=1}^{N} a_i \frac{e^{-jk_0 r_i}}{r_i} + \sum_{i=1}^{N} a_i' \frac{e^{-jk_0 r_i'}}{r_i'} \tag{18}$$
where
$$r_i = \sqrt{\rho^2 + (z + z' - jb_i)^2}. \tag{19}$$

The procedure of two-path approximation is similar to the two-level DCIM, as in [6]. However, the purpose of the two-path DCIM in this paper is totally different from the two-level approximation in [6]. The purpose of [6] is to save the CPU time, but the goal in this paper is to find a straightforward method to improve the accuracy of the DCIM in the far-field region without any loss of performance in the near-field region. We can break the path C_{12} in two segments and sample them with different rates similar to [6] to save the CPU time, but it is not our focus in this paper.

From (18), we can see that the spatial-domain GF can be approximated by a sum of uniform expressions of complex exponentials, which is similar to the GF for a homogeneous media. No other terms are necessary and there is only one GF for all the various horizontal distances. Simulation results in Section IV show the accuracy of (18) both in the near- and far-field regions.

IV. Numerical Results

In the first example, we use the same microstrip problem as used in Section III. A general multilayered case is shown in the second example.

When γ is first chosen according to the requirement of the problem, the length of the path C_{12} is accordingly set as T_0/γ. T_o is chosen as 7.5 in this example. The sampling step on C_{12} is chosen as $dt = 0.1$. Note that although dt is fixed for different γ, the sampled points are automatically more dense, as C_{12} is closer to the singularities, due to the relation in (15). Since the DCIs obtained on C_{12} should contain the variation information on C_{11}, the computation of the third step of the DCIM on C_{11} is trivial. $dt = 10$ is enough to apply the MPM on C_{11}.

A threshold tol can be set in the MPM to control the accuracy. The first step of the MPM is to do the singular value decomposition (SVD) of a Hankel matrix built by the sampled data of $\tilde{G}(k_\rho)$ [11]. We choose the biggest M singular values, which are larger than $tol \cdot \sigma_{\max}$ where $\sigma_{\max}$ is the largest singular value. M is also the number of exponentials. In this paper, for the main computation of the MPM on C_{12}, we set $tol = 10^{-10}$. For the MPM on C_{11}, $tol = 10^{-3}$ because most singular values are zeros on this path.

The values of γ, the number of singular values, how far along the horizontal direction $\rho_{\max}$ can be reached accurately for the spatial-domain GF, and the CPU times in a P4 2.8-GHz PC are listed in Table I. $\rho_{\max}$ is calculated by analyzing the normalized error of the DCIM compared with the accurate numerical integration. It is obtained when the normalized error is less than

TABLE I
PERFORMANCES OF DCIM FOR DIFFERENT γs

γ	M on C_{12}	M on C_{11}	$\rho_{\max}$	CPU-time (sec)
[5]	19	0	4.4 λ	0.47
0.200	54	5	16.9 λ	0.79
0.100	99	6	33.6 λ	4.84
0.050	185	7	69.5 λ	33.9
0.025	385	8	125 λ	256.0
0.017	546	8	> 160 λ	932.1

5×10^{-2}, which is small enough for the matrix element of the MoM in most applications. We can choose a different threshold of the normalized error and $\rho_{\max}$ will change accordingly, but the relevant sorting order of the forth column of Table I will not change. λ in Table I is the wavelength in free space. The first line is the situation for the traditional DCIM in [5] (without singularity extrapolation) along the path on C_0', as in Fig. 1 (in this example, T_0 is chosen as 7.5). The other five lines are the results of the new DCIM along the path on C_{12} and C_{11}, as shown in Fig. 5. Note that with $\gamma = 0.2$, we can easily obtain an accurate spatial GF up to 16.9 λ, which is larger than the largest horizontal distance provided by all the previous papers. The CPU time used in this case is 0.32 s longer than that in [5], but still less than 1 s. Smaller γ are listed for reference when extremely large structures [13]–[15] are going to be analyzed in multilayered media. Note that although the computational load of the new DCIM is approximately equal to $O[(1/\gamma)^3]$, the CPU time used for the computation of the GF is still negligible compared with the matrix solving part in the MoM [14].

Fig. 7 shows the plots of G_q for two values of γ together with the accurate results. They are both accurate with small ρ and go further along ρ compared with the traditional DCIM in Fig. 4.

Fig. 8 shows the plots of G_{xx}^A. The relationship between γ and $\rho_{\max}$ remain similar as for G_q in Table I; hence, the performance of either G_q or G_{xx}^A is decided by γ, which is easy to control. The difference is that the number of exponentials M on C_{12} in G_{xx}^A is smaller than that in G_q. The reason for this difference is that the spectral kernel G_{xx}^A contains only one singularity instead of two. However, this difference does not affect the performance. The new direct DCIM is robust.

As a more general example, we take the same five-layer microstrip structure in [7, Fig. 1]. The source point is in the second layer and the field point is in the fourth layer. The results in [7] are accurately obtained both in the near and far field by the proposed DCIM without any extrapolation of the quasi-static static or surface-wave terms, which is shown in Fig. 9. Note that, to apply the proposed DCIM, the two paths of k_z in Fig. 5(a) should be in the layer with the minimum ε_r (usually the free-space layer). By doing this, path C_{11} and C_{12} will be constrained in the same Riemman sheet and path C_{11} will not cross the branch point.

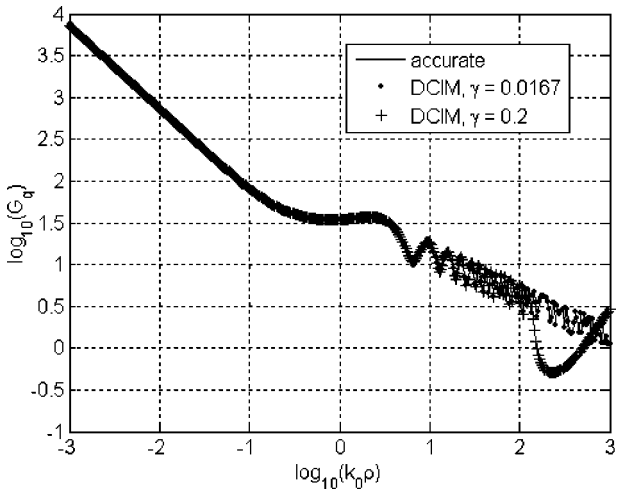

Fig. 7. Spatial-domain G_q obtained by direct DCIM.

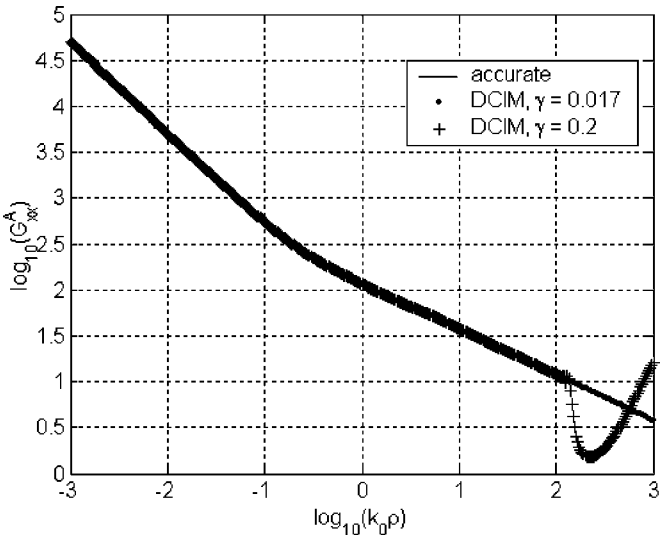

Fig. 8. Spatial-domain G_{xx}^A obtained by direct DCIM.

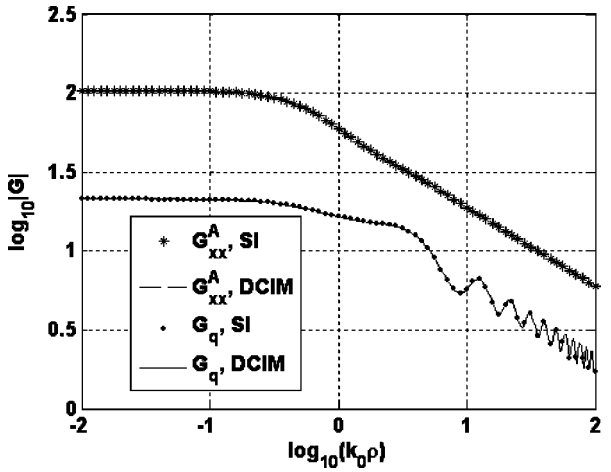

Fig. 9. Spatial-domain G_{xx}^A for a general multilayered microstrip. $\gamma = 0.2$ for the proposed DCIM.

V. Conclusions

A new direct DCIM has been introduced in this paper. Compared with the traditional DCIM, this method does the reverse before applying the MPM: it tries to include more variations of the spectral kernel and, hence, more information about the singularities. This method is feasible due to the powerful features of the MPM. It is implemented by choosing a novel path nearer to the singularities. The spatial-domain GF obtained by this method is accurate both in the near- and far-field regions, and the performance is robust according to the choice of γ. The spatial-domain GF is calculated using the same expression of a sum of spherical waves, which is suitable for numerical calculation by the computer. No quasi-static or surface-wave terms are extracted because they are not necessary.

Acknowledgment

The authors would thank the reviewers and Dr. F. Ling, Cadence Design Systems Inc., Tempe, AZ, for their valuable suggestions and comments.

References

[1] R. F. Harrington, *Field Computation by Moment Methods*. New York: Macmillan, 1968.

[2] A. Sommerfeld, *Partial Differential Equations in Physics*. New York: Van Nostrand, 1990.

[3] T. K. Sarkar, "Analysis of arbitrarily oriented thin wire antenna arrays over imperfect ground planes," Ph.D. dissertation, Dept. Elect. Eng. Comput. Sci., Syracuse Univ., Syracuse, NY, 1975.

[4] K. A. Michalski, "Extrapolation methods for Sommerfeld integral tails," *IEEE Trans. Antennas Propag.*, vol. 46, no. 10, pp. 1405–1418, Oct. 1998.

[5] Y. L. Chow, J. J. Yang, D. G. Fang, and G. E. Howard, "A closed-form spatial Green's function for the thick microstrip substrate," *IEEE Trans. Microw. Theory Tech.*, vol. 39, no. 3, pp. 588–592, Mar. 1991.

[6] M. I. Aksun, "A robust approach for the derivation of closed-form Green's functions," *IEEE Trans. Microw. Theory Tech.*, vol. 44, no. 5, pp. 651–658, May 1996.

[7] F. Ling and J.-M. Jin, "Discrete complex image method for Green's functions of general multilayer media," *IEEE Microw. Guided Wave Lett.*, vol. 10, no. 10, pp. 400–402, Oct. 2000.

[8] Y. Ge and K. P. Esselle, "New closed-form Green's functions for microstrip structures—Theory and results," *IEEE Trans. Microw. Theory Tech.*, vol. 50, no. 6, pp. 1556–1560, Jun. 2002.

[9] S.-A. Teo, S.-T. Chew, and M.-S. Leong, "Error analysis of the discrete complex image method and pole extraction," *IEEE Trans. Microw. Theory Tech.*, vol. 51, no. 2, pp. 406–413, Feb. 2003.

[10] Y. Hua and T. K. Sarkar, "Generalized pencil-of-function method for extracting poles of and EM system from its transient response," *IEEE Trans. Antennas Propag.*, vol. 37, no. 2, pp. 229–234, Feb. 1989.

[11] T. K. Sarkar and O. Pereira, "Using the matrix pencil method to estimate the parameters of a sum of complex exponentials," *IEEE Antennas Propag. Mag.*, vol. 37, pp. 48–55, Feb. 1995.

[12] K. A. Michalski and J. R. Mosig, "Multilayered media Green's functions in integral equation formulations," *IEEE Trans. Antennas Propag.*, vol. 45, no. 3, pp. 508–519, Mar. 1997.

[13] B. M. Kolundzija and A. R. Djordjevic, *Electromagnetic Modeling of Composite Metallic and Dielectric Structures*. Boston, MA: Artech House, 2002.

[14] M. Yuan and T. K. Sarkar, "Electrically large structures in WIPL-D," in *2005 IEEE/ACES Int. Conf.*, Honolulu, HI, Apr. 3–7, 2005, pp. 82–85.

[15] B. M. Kolundzija, J. S. Ognjanovic, T. K. Sarkar, and R. F. Harrington, *WIPL, Software for Electromagnetic Modeling of Composite Wire and Plate Structures*. Norwood, MA: Artech House, 1995.

Mengtao Yuan (S'02) was born in Chongqing, China. He received the B.S. degree in information and electronic engineering and M.S. degree in information and communication system from Zhejiang University, Hang Zhou, China, in 1999 and 2002, respectively, and is currently working toward the Ph.D. degree in electrical engineering at Syracuse University, Syracuse, NY.

Since 2002, he has been a Research Assistant with Syracuse University. His current research interests include electromagnetic computation in multilayered media, time- and frequency-domain CEM, efficient solvers for electrically large structures, circuit and antenna design, and signal processing in communications.

Tapan K. Sarkar (S'69–M'76–SM'81–F'92) received the B.Tech. degree from the Indian Institute of Technology, Kharagpur, India, in 1969, the M.Sc.E. degree from the University of New Brunswick, Fredericton, NB, Canada, in 1971, and the M.S. and Ph.D. degrees from Syracuse University, Syracuse, NY, in 1975.

From 1975 to 1976, he was with the TACO Division, General Instruments Corporation. From 1976 to 1985, he was with the Rochester Institute of Technology, Rochester, NY. From 1977 to 1978, he was a Research Fellow with the Gordon McKay Laboratory, Harvard University, Cambridge, MA. He is currently a Professor with the Department of Electrical and Computer Engineering, Syracuse University. His current research interests deal with numerical solutions of operator equations arising in electromagnetics and signal processing with application to system design. He has authored or coauthored over 280 journal papers and numerous conference papers and 32 chapters in books and 15 books, including *Iterative and Self Adaptive Finite-Elements in Electromagnetic Modeling* (Artech House, 1998), *Wavelet Applications in Electromagnetics and Signal Processing* (Artech House, 2002), *Smart Antennas* (Wiley, 2003), and *History of Wireless* (Wiley, 2005). He is on the Editorial Board of the *Journal of Electromagnetic Waves and Applications* and *Microwave and Optical Technology Letters*.

Dr. Sarkar is a Registered Professional Engineer in the State of New York. He was an associate editor for feature articles of the *IEEE Antennas and Propagation Society Newsletter* (1986–1988). He is a member of Sigma Xi and International Union of Radio Science Commissions A and B. He is currently a member of the IEEE Electromagnetics Award Board and an associate editor for the IEEE Transactions on Antennas and Propagation. He is the vice president of the Applied Computational Electromagnetics Society (ACES). He was the chairman of the Intercommission Working Group of the International URSI on Time Domain Metrology (1990–1996). He was a distinguished lecturer for the IEEE Antennas and Propagation Society (2000–2003). He was the recipient of the 1979 Best Paper Award of the IEEE Transactions on Electromagnetic Compatibility and at the 1997 National Radar Conference. He was the recipient of the 1996 College of Engineering Research Award and the 1998 Chancellor's Citation for Excellence in Research at Syracuse University. He was the recipient of one of the 1977 Best Solution Awards presented at the Rome Air Development Center (RADC) Spectral Estimation Workshop. He received the title of Docteur Honoris Causa from the Universite Blaise Pascal, Clermont Ferrand, France, in 1998 and from the Politechnic University of Madrid, Madrid, Spain, in 2004. He was also the recipient of the 2000 Medal of the Friend of the City of Clermont Ferrand, France.

Magdalena Salazar-Palma (M'89–SM'01) was born in Granada, Spain. She received the degree and Ph.D. degree in ingeniero de telecomunicación from the Universidad Politécnica de Madrid, Madrid, Spain.

She is currently a Catedrático (Full Professor) with the Departamento de Teoría de la Señal y Comunicaciones (Signal Theory and Communications), Escuela Politécnica Superior (College of Engineering), Universidad Carlos III de Madrid, Madrid, Spain. She has authored four books, 20 contributions for chapters and articles in books, 48 papers in international scientific journals, and 172 papers in international conferences, symposiums, and workshops, 13 contributions for academic books and notes, 56 papers in national conferences, and over 75 project reports, short course notes, etc. She has delivered numerous invited presentations, lectures, and seminars. She has lectured in several short courses, some of them in the frame of Programs of the European Community. She has participated at different levels (researcher or director) in a total of 62 projects and contracts, financed by international, European, and national institutions and companies. She has developed her research in the areas of electromagnetic-field theory; computational and numerical methods for microwave passive components and antenna analysis; network and filter theory and design; and design, simulation, optimization, implementation, and measurement of microwave circuits both in waveguide and integrated (hybrid and monolithic) technologies. She has been a member of the editorial board of two scientific journals.

Dr. Salazar-Palma is member of the Technical Program Committee of several international and national symposiums and reviewer for different international scientific journals, symposiums, and editorial companies. She has assisted the Comisión Interministerial de Ciencia y Tecnología (Spain National Board of Research) in the evaluation of projects. She has also served in several evaluation panels of the Commission of the European Communities. She has been associate editor for the IEEE ANTENNAS AND WIRELESS PROPAGATION LETTERS. Since 1989, she has served the IEEE under different volunteer positions: vice chairperson and chairperson of the IEEE Spain Section Antennas and Propagation Society (AP-S)/Microwave Theory and Techniques Society (MTT-S) Joint Chapter, chairperson of the IEEE Spain Section, member of the IEEE Region 8 Committee, member of the IEEE Region 8 Nominations and Appointments Subcommittee, chairperson of the IEEE Region 8 Conference Coordination Subcommittee, chairperson of the IEEE Women in Engineering (WIE) Committee, liaison between the IEEE WIE Committee and the IEEE Regional Activities Board, and member of the IEEE Ethics and Member Conduct Committee. She is currently the membership development officer of the IEEE Spain Section, a member of the IEEE WIE Committee and a member of the IEEE AP-S Administrative Committee (AdCom). She was the recipient of two individual research awards.